Noninvasive In Vivo Detection of Prognostic Indicators for High-Risk Uveal Melanoma

Ultrasound Parameter Imaging

D. Jackson Coleman, MD,[1,2] Ronald H. Silverman,[1,2] Mark J. Rondeau,[1,2] H. Culver Boldt, MD,[3] Harriet O. Lloyd,[1] Frederic L. Lizzi,[4] Thomas A. Weingeist, MD,[3] Xue Chen, MD,[5] Sumalee Vangveeravong, MD,[5] Robert Folberg, MD[5]

Purpose: Primary malignant melanoma of the choroid and ciliary body has traditionally been treated without histologic staging, using purely clinical indicators. The presence of extravascular matrix patterns (EMP) in histologic sections of uveal melanoma has been shown to be an independent indicator of metastatic risk. These patterns are of a dimension and physical composition that are likely to be detected with ultrasound backscatter analysis. Our aim was to determine whether ultrasound parameter imaging could detect the presence of EMP at a diagnostically significant level for treatment staging and for planning investigational studies of therapeutic modalities.

Design Prospective, masked ultrasound–pathologic correlative study.

Participants: One hundred seventeen patients diagnosed with previously untreated choroidal melanoma were scanned within 2 weeks before enucleation.

Methods: Tumors were evaluated histologically and divided into high-risk and low-risk groups on the basis of the presence of 2% or more histologic cross-sectional area composed of EMP patterns. Digital ultrasound data were processed to generate parameter images representing the size and concentration of ultrasound scatterers. Histologic and ultrasound images and data were correlated, and linear and nonlinear statistical methods were used to create multivariate models for noninvasive differentiation of high-risk and low-risk tumors.

Main Outcome Measures: Presence or absence of high-risk EMP and associated ultrasound parameter classification models.

Results: Of the 117 tumors, 69 were classified as low risk, and 48 were classified as high-risk with histologic analysis. A classification that used ultrasound parameter image features with linear discriminant analysis could correctly identify 79.5% of cases retrospectively and 75.2% of cases by use of cross-validation, an estimate of prospective classification ability. By use of a more powerful classification technique (support vector machine), 93.1% of cases were correctly classified retrospectively. With a cross-validation procedure, 80.10% of cases were correctly classified.

Conclusions: Ultrasound can be used noninvasively to classify tumors into high-risk and low-risk groups by detecting the presence of EMP patterns. By the use of previous studies that compared the histologic presence of EMP patterns with patient survival, estimates of hazard rates associated with ultrasound risk groups can be made. The noninvasive ultrasound classification is potentially useful as a prognostic variable and as a tool for stratification of patient populations for tumor treatment evaluation. *Ophthalmology 2004;111:558–564 © 2004 by the American Academy of Ophthalmology.*

Primary uveal melanoma is a rare neoplasm. Its incidence rate is very low at approximately 6 new cases per million per year.[1] It is also an uncharacteristic ocular condition because of its life-threatening potential. Most cases of uveal melanoma continue to be diagnosed and treated based

Originally received: February 24, 2003.
Accepted: June 23, 2003. Manuscript no. 230104.

[1] Department of Ophthalmology, Weill Medical College of Cornell University, New York, New York.

[2] The Margaret M. Dyson Vision Research Institute, New York, New York.

[3] Department of Ophthalmology and Visual Sciences, University of Iowa, Iowa City, Iowa.

[4] Biomedical Engineering Directorate, Riverside Research Institute, New York, New York.

[5] Department of Pathology, University of Illinois–Chicago, Chicago, Illinois.

Supported by National Institutes of Health grants (EB00238, EY10457), Research to Prevent Blindness, Inc., and the St. Giles Foundation.

The authors have no commercial interest in this study.

Correspondence to D. Jackson Coleman, MD, Department of Ophthalmology, Weill Medical College of Cornell University, A-856, 1300 York Ave., New York, NY 10021. E-mail: djceye@aol.com.

ISSN 0161-6420/04/$–see front matter
doi:10.1016/j.ophtha.2003.06.021

purely on clinical information using size, appearance, and location, in contrast to most other cancers that are staged histologically before treatment. Prognostic information for uveal melanoma is available by use of histologic, cytologic, and cytogenetic features of tumor material obtained through fine-needle aspiration biopsy, but the issue of safely obtaining a representative sample of this material for analysis remains in question.[1–4] Various types of noninvasive imaging also have been used for the differential diagnosis of ocular tumors, as well as to obtain prognostic information.[5–8] To provide rational therapy for uveal melanoma that balances the risk of loss of sight with the possible loss of life, prognostic information beyond clinical staging needs to be incorporated into therapeutic decision making.

In this study, we describe a noninvasive staging approach for uveal melanoma on the basis of the correlation between the presence of extravascular matrix patterns (EMP), a prognostic histologic feature, and the ultrasound scattering features of these tumors. Previous work in retrospective survival studies showed that certain ultrasound scattering characteristics of uveal melanoma are associated with increased risk of death from metastasis.[9,10] In these studies, the relationship between ultrasound scattering and survival risk was made using a correlation between tumor cell type (modified Callendar classification) and ultrasound parameters. A relationship between ultrasound parameters and the presence of EMP features was found in a preliminary study of 40 patients who are included in this study.[11]

Folberg et al[12] have demonstrated that specific histologic patterns in uveal melanoma are associated with increased risk of metastasis. This finding has been subsequently confirmed by other groups.[13–16] The EMP patterns (cross-linking parallel structures, arc, loops, and networks of loops) are generated in vitro only by aggressive uveal melanoma cells; nonaggressive cells do not generate these patterns.[17,18] Therefore, the presence of these patterns histologically is associated with an aggressive tumor cell phenotype. Although these patterns are not blood vessels,[18] they connect to vessels.[17–19] Fluid is transported through these patterns formed by aggressive uveal melanoma cells in vitro,[17,18] in animal models of melanoma,[20,21] inflammatory breast cancer,[22] and in human uveal melanoma tissue.[18] Recent work by Mueller et al[23]has shown that dye perfusion through EMP can be demonstrated in vivo and is associated with the risk of continued growth in these tumors.

The relationship between the microstructure of tissue and the appearance of tissue on ultrasonography is complex. The patterns seen in ultrasonograms are caused by local fluctuations in density and elasticity of the tissue. These differences in density and elasticity give rise to the ultrasound scattering that is responsible for gray-scale texture of a B scan or the A-scan amplitude spikes. The internal structure of uveal malignant melanoma on B-scan ultrasound is typically seen as a relatively homogeneous gray-scale pattern that is not specifically diagnostic. Although A-scan pattern analysis can allow for differentiation between primary melanoma and metastatic tumors, as well as between some spindle type and mixed and epithelioid type tumors, it cannot be used to reliably subclassify melanoma.

We have extended the analysis of ultrasound data beyond amplitude displays such as B scan and A scan by examining the underlying frequency characteristics of the ultrasound signal. Mathematical modeling of ultrasound–tissue interaction shows that the frequency content of an ultrasound signal can be used to estimate the relative size and concentration of ultrasound scatterers that are smaller than the typical specular reflector such as the surface of the tumor.[24,25]

This study uses images of the estimates of size and concentration of ultrasound scattering elements to identify high-risk and low-risk melanomas as defined by the percentage of EMP seen histologically. The cross-sectional dimensions of EMP range from 14 to 116 μm (median, 43 μm) in width and 30 to 157 μm (median, 70 μm) in length.[26] These dimensions are within the scattering range sensed by our 10-MHz center frequency ultrasound systems. In addition to being in the correct size range, the EMP is composed of dense structural proteins, such as laminin and collagen, that efficiently scatter ultrasound.

Materials and Methods

This study adhered to the tenets of the Declaration of Helsinki and was approved by the institutional review boards of the University of Iowa Hospitals and Clinics (UI), the University of Illinois-Chicago, and the Weill Medical College of Cornell University.

All patients in this study were diagnosed clinically as having choroidal melanoma. Patients enrolled in this study either did not qualify for or refused entry into the Collaborative Ocular Melanoma Study. None of the tumors in our study had been treated previously with radiation or other modalities. All ultrasound scanning was performed at UI within a 2-week period before enucleation. A Sonovision STT-100 (Sonocare, Saddle River, NJ), equipped with a broadband 10-MHz mechanical sector scan probe and a 50-MHz analog-to-digital converter, was used for ultrasound data acquisition. Data from at least 5 scans that matched the planned histologic section planes were recorded during each examination. Radiofrequency echo data collected at UI were sent to Weill Medical College of Cornell University for analysis. Histologic analysis of eyes enucleated at UI was performed at University of Illinois-Chicago.

Eyes were first fixed in 10% neutral buffered formalin for at least 48 hours before sectioning and then opened in the presence of the investigator who had performed the ultrasonography. A gross-pathology protocol designed for precise clinicopathologic correlations of eyes removed for uveal melanoma[27] was used to ensure that section planes were taken from the areas of the tumor imaged by ultrasound. Paraffin-embedded tissue was sectioned at 5 μm and stained with hematoxylin–eosin and periodic acid–Schiff stain without hematoxylin counterstaining, using permanganate bleaching[26]if necessary. Photomicrographs of histologic sections stained with the periodic acid–Schiff stain were then digitized.[28] Regions on the digitized histologic sections containing prognostically significant EMP patterns were color coded[29] to represent arcs and arcs with branching (green), parallels with cross-linking (yellow), and loops and networks (red). Colorized information was encoded in the form of a digital overlay, so that the original histologic section underlying the color coding remains accessible. Tumor location was documented along with largest basal diameter.

Mehaffey et al[30] suggested criteria for classification of uveal melanoma into high-risk and low-risk groups on the basis of the presence of at least 2% of the tumor's cross-sectional area being composed of high-risk EMP patterns (parallels with crosslinks,

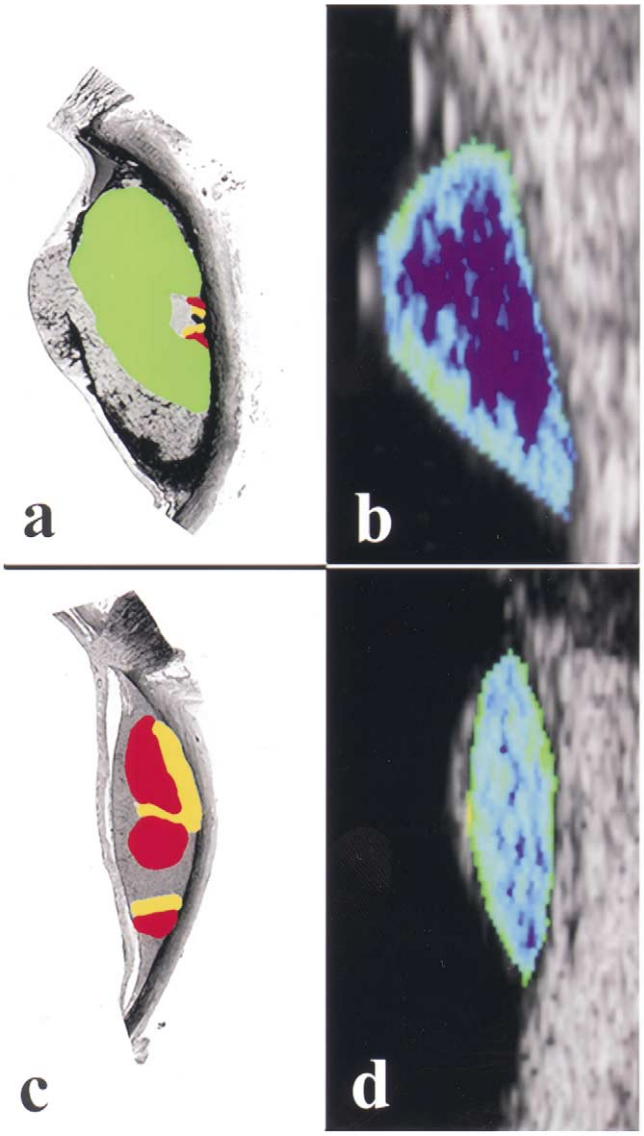

Figure 1. Representative low-power histologic sections of 2 high-risk tumors (>2% of cross-sectional histologic area) with color overlay **(A, C)**. Areas in red denote the presence of closed loops and networks. Areas in green denote arcs and arcs with branching. Areas in yellow denote parallel with cross-linking extravascular matrix (EMP) features. Companion acoustic concentration images **(B, D),** with darker colors representing lower acoustic concentration are shown. There is good spatial congruence between EMP features and areas of low scatterer concentration in **A** and **B**, and less so in **C** and **D**. This underscores the statistical nature of the classification procedure, which relies on a set of both global and local properties of parameter images.

arcs, loops, and networks). We used the same criteria to divide our database into 2 histologic risk groups.

Ultrasound parameter images were generated using power spectrum analysis.[6,31–33] In these images, the pixel values were recoded to represent either scatterer diameter or scatterer concentration instead of the gray-scale value representing echo amplitude in the conventional B-mode image. To obtain parameter images of the tumors, B-mode images were digitally reconstructed from

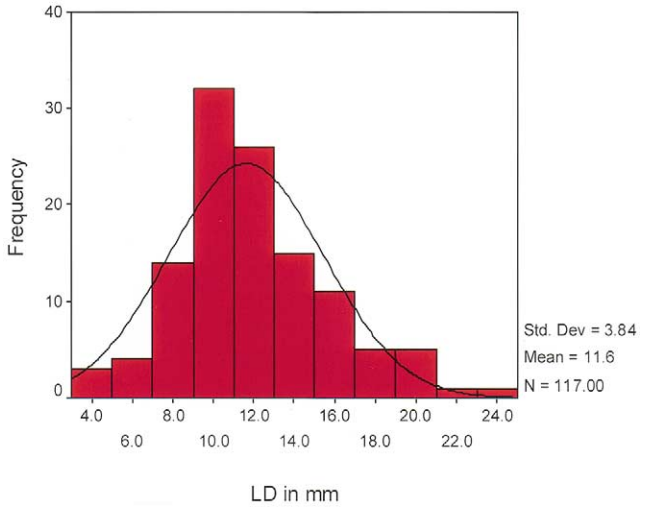

Figure 2. A bar plot showing the distribution of maximal basal tumor dimension as measured in histologic sections. The normal distribution for this data set is given by the solid line. LD = largest dimension.

acquired radiofrequency data and the tumor outlined manually. The tumor area was then automatically divided into 3 regions of equal area, representing the anterior, posterior, and core of the tumor. The outline was used to specify the scan-line segments to be analyzed. We analyzed the tumor using a sliding-window fast Fourier transform technique in which successive overlapping 0.5-mm × 0.5-mm analysis regions were analyzed across the demarcated area of the tumor. The resultant normalized power spectra were analyzed with a linear least-squares fit providing values of spectral slope (dB/MHz) and intercept (dB). The slope is a measure of amplitude dependence of frequency, and the intercept (interpolated amplitude at 0 MHz) is a measure of amplitude independent of frequency. A mathematical model of acoustic backscatter by stochastic distributions of scatterers (Gaussian isotropic autocorrelation function) was then used to estimate effective scatterer diameter and acoustic concentration. These methods have been previously described in greater detail.[5,6,9–11,32–34] Figure 1

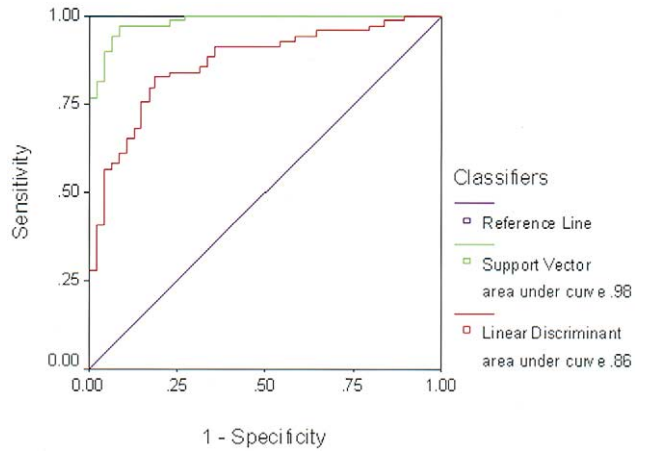

Figure 3. The receiver operator characteristic curve analysis for the linear discriminant analysis and support vector machine in terms of retrospective performance. The area under the curve, a measure of the performance of a classifier, was 0.866 for the linear discriminant analysis and 0.983 for the support vector machine.

shows low-powered histologic sections, with color overlays denoting regions with EMP along with companion acoustic concentration images.

Statistical Analysis

Statistical analyses were performed with SPSS version 11 (SPSS, Inc, Chicago, IL) and public domain software for Support Vector Machine and receiver operator characteristic (ROC) convex hull analysis. After testing for differences in the variance of acoustic parameters between histologic risk groups, Student's *t* tests (independent samples, 2-tailed) were applied to identify statistically significant differences in parameters between the 2 groups. When variance values did not differ significantly ($P>0.05$), pooled variance values were used in the *t* tests; otherwise, the variances of the individual groups were used. These parameters included the mean values of scatterer size and acoustic concentration within the tumors as a whole and each of the 3 subregions and the standard deviations of these parameters (representing spatial variability). We also compared the percentage of the tumor area composed of parameterized pixels representing small scatterers (<64 μm) or low-scatterer concentration (< -20 dB). In addition to parameters derived directly from statistics of the scatter size and concentration images, we also used discrete 2-dimensional wavelet transform techniques to examine the parameter images' statistical properties.[35] This technique has been shown to be useful in examining spatially localized and oriented differences in signal content in diagnostic imaging.[36,37] For this study, we examined the variance of orientation details at different resolution levels for statistically conditioned acoustic concentration images.

Stepwise linear discriminant analysis (a standard linear classifier) was performed to determine the separability of the high and low EMP risk groups on the basis of ultrasound parameters. The variable entry criterion was a *P* value of 0.05 or less. The a priori values for group membership were set proportional to group size. We also used a machine learning classifier, the support vector machine. The rationale for this was 2-fold: the support vector machine allows model complexity or overfitting to be controlled along with error minimization, so that real world performance is easily evaluated.[38,39] The support vector machine has excellent, possibly optimal, empirical performance in a wide variety of classification tasks.[40–42] Receiver operator characteristic analysis, the standard measure of the diagnostic ability of a test, was used to compare the performance of the classifiers.[43] In addition, to further analyze the real-world performance of the classifiers, we used the ROC convex hull method. This allowed us to examine the effect that a difference in the number of high-risk versus low-risk patients (class distribution) might have on classifier performance. In addition, this technique was used to examine several cost-minimization scenarios in which the relative "cost" of a false-positive or false-negative result was varied for specific groups of patients and treatment options.[44,45]

Results

The location characteristics for the study population are shown in Table 1. More than 25% of the tumors in this study have some ciliary body involvement. The size distribution in terms of basal dimension is shown in Figure 2. The mean basal dimension of 11.62 mm for the study population is similar to that of patients enrolled in the Collaborative Ocular Melanoma Study (11.4 mm).[46] *T* test results comparing acoustic parameters between histologic risk groups identified statistically significant univariate differences between the histologic prognostic groups for acoustic parameters determined either for the tumor as a whole or within specific spatial regions. The most consistent finding is the significance of scatterer concentration–related variables. Variables associated with scatterer diameter were generally of less significance, but their levels in the anterior of the tumor (where attenuation, a confounding factor for scatterer size estimates, would least affect their values) did reach or approach significance.

Table 1. Location of Uveal Melanomas

Location	Number of Patients	Percentage
Choroid	86	73.5
Choroid and ciliary body	27	23.1
Ciliary body	4	3.4
Total	117	100.0

Variables with univariate significance were used as input to the stepwise linear discriminant analysis. The stepwise analysis produced a model that included 6 acoustic parameters: (1) ultrasound scatterer concentration in the posterior aspect of the tumor; (2) the percentage of posterior low-concentration scatterers; (3) the percentage of anterior small to medium-sized scatterers; (4) core region scatterer concentration standard deviation; (5) the variance of the vertical orientation at detail level 2; and (6) the variance of the vertical orientation at detail level 3. Three of the model parameters are associated with scatterer concentration, 2 with the vertical wavelet orientation, and 1 with the size of the scattering elements.

The overall percentage of correctly classified cases for the linear discriminant model (which represent a single point on the ROC curve) was 79.5%, with 76.8% of histologic low-risk cases correctly identified, and 83.3% of high-risk cases identified. Leave-one-out cross-validation analysis (in which each case from the database is successively treated as an unknown) resulted in a decrease of 4.3% in the overall percentage of correctly identified cases relative to retrospective analysis. The overall classification results are given in Table 2.

We used the variables selected by the linear discriminant analysis to develop our support vector machine classification model. Support vector machine software with parameter optimization methods found both linear and nonlinear support vector machine models with better performance than the linear discriminant models. We identified a nonlinear model support vector machine with minimal complexity that had an overall percentage of correctly classified cases (which represent a single point on the ROC curve) of 93.15%, with 88.4% of histologic low-risk cases correctly identified, and 97.9% of high-risk cases identified retrospectively. The leave-one-out cross-validation analysis resulted in an estimated prospective performance of 80.1%, a decrease of 13% in the overall number of correctly classified cases relative to retrospective analysis. The overall classification results are given in Table 3.

In addition to providing improved overall retrospective and estimated prospective performance, model performance in terms of false-negative results in the high-risk group is reduced by 50% with the support vector machine classification model.

Receiver operator characteristics plot area under the curve defines expected accuracy of the classifier and can be defined for the retrospective classifiers. The area under the ROC curves was 0.866 for the linear discriminant analysis and 0.983 for the support vector machine classifier (Fig 3). Receiver operator characteristics convex hull analysis confirmed that the support vector machine classifier provided the most robust performance over a wide class distribution and error cost range outperforming linear discriminant analysis.

Table 2. Classification Results for Linear Discriminant Analysis Model

Classification	Percent of Cases Correctly Classified	Predicted Group Membership	*Low Risk*	*High Risk*	Total
Retrospective	79.5	Low risk	53	16	69
		High risk	8	40	48
		% Low risk	76.8	23.2	100.0
		% High risk	16.7	83.3	100.0
Cross-validated	75.2	Low risk	50	19	69
		High risk	10	38	48
		% Low risk	72.5	27.5	100.0
		% High risk	20.8	79.2	100.0

Discussion

Fear of losing vision, coupled with the instinctive fear of loss of life, poses terrible dilemmas for patients with choroidal or ciliary body melanomas and for their physicians. Two polls conducted by the Gallup Organization asked the following question to Americans: "What disease do you fear most?" Before public awareness of AIDS and Alzheimer's disease, the most feared disease was cancer, and the second most feared disease was blindness (The Gallup Organization, Inc.; "Public knowledge and attitudes concerning blindness." A survey sponsored by Research to Prevent Blindness, Inc., New York, October 1965, April 1976, unpublished data). If ophthalmic oncologists can preserve vision without increasing the risk to the patient's life, most patients will opt for a treatment that does not require removal of the eye. The preliminary results from the Collaborative Ocular Melanoma Study have indicated that radiation and enucleation have essentially the same risk of death.[47]

Patients are currently stratified into treatment groups on the basis of tumor size and location.[48] Although ophthalmologists have used intraocular fine-needle biopsies to discriminate between melanomas and lesions that simulate melanomas clinically with a high level of accuracy,[48–50] uveal melanomas are composed of heterogeneous cell populations. At least 2 studies indicate that intraocular needle biopsies might not extract material that is representative of the tumor.[50,51] Unlike fine-needle aspiration biopsies performed at other body sites in which the surgeon or pathologist makes multiple passes into the lesion from different angles to ensure a representative sampling of the lesion,[52] the ophthalmic oncologist typically makes only 1 pass into the lesion to avoid disruption of anatomic structures critical for vision.[48,51] There is no indication that fine-needle biopsy would ever be able to reliably correlate with the presence of EMP, because the entire tumor would need to be evaluated.

The use of confocal indocyanine green angiography to identify the presence of EMP in tumors with a median basal dimension of 7.00 mm has also been reported.[23] The angiographic technique seems useful in smaller size tumors located posterior to the equator. The typical medium size tumor in our study, with choroidal involvement only, extends in part beyond the equator.

Ultrasound is a safe noninvasive procedure that can assess ocular tumors regardless of location and media clarity. In addition, it can be performed in multiple planes throughout the tumor in a fashion similar to the pathologist's serial histologic sectioning. Interestingly, when prognostically significant matrix-rich patterns are present in a tumor, they tend to be distributed throughout the tumor mass in different planes,[53]increasing the likelihood of pattern detection by a noninvasive imaging technique.

Previous studies have shown acoustic backscatter properties are correlated with survival in patients with uveal malignant melanoma.[9,10] Similarly, the presence of matrix-rich patterns is an independent risk factor for metastatic spread.[12] This study shows that acoustic backscatter spectrum correlate with the presence of these histologic patterns discriminating between lethal and less lethal tumors.

The spatial conformation and distribution of matrix-rich patterns may be complex, and acoustic backscatter depends on the orientation of scatterers in addition to their number and size. Our current working hypothesis concerning the 3-dimensional configuration of these patterns is that the EMP surrounds spheroidal nests of tumor cells (Maniotis

Table 3. Classification Results for Support Vector Machine Model

Classification	Percent of Cases Correctly Classified	Predicted Group Membership	*Low Risk*	*High Risk*	Total
Retrospective	93.15	Low risk	61	8	69
		High risk	1	47	48
		% Low risk	88.4	11.6	100.0
		% High risk	2.1	97.9	100.0
Cross-validated	80.1	Low risk	50	19	69
		High risk	5	43	48
		% Low risk	72.5	27.5	100.0
		% High risk	10.5	89.5	100.0

AJ, personal communication cited by Barinaga[54]). In this case, the orientation of matrix and tumor cells would be nearly isotropic, and current classifier should provide good performance in individual tumors. However, if the appearance of loops on 2-dimensional histologic sections reflects matrix deposition around elliptical or cylindrical tumor cell clusters, tumor backscatter might be more dependent on the angle of the ultrasound beam relative to the scatterers. This would also be the case with backscatter properties associated with matrix-rich cross-linking parallel patterns. If these patterns are oriented perpendicular to the beam axis, backscatter will be increased, and if patterns are parallel, backscatter will be reduced. The importance of the extracellular matrix and its orientation on backscatter in myocardial tissue was recently described.[55] Therefore, a more complete understanding of the 3-dimensional distribution of these EMP patterns might provide avenues to enhance ultrasonic detection and classification of ocular tumors even greater than already shown by our data.

The ability to obtain prognostic information regarding uveal melanoma noninvasively and thus to stratify tumors into risk groups can be of benefit both to patients and to investigators conducting treatment studies. If patients entering a survival study are divided into risk groups of known low and high hazard rates, conclusions might be reached with fewer subjects and in less time than if all patients were treated as 1 group. For example, consider the design of a prospective randomized evaluation of uveal melanoma treatment. If published hazard rates are used,[24,47,56] and study patients have the same class distribution seen in this study, a medium to large prospective trial with equivalent statistical power could be performed with a shorter accumulation period, fewer numbers of subjects, and a shorter total study duration than if all patients were considered to have equivalent risk entering the study.

The ultrasound classification can provide the individual patient and physician with a rational basis for decisions on therapy and for clinical monitoring for metastasis. Patients treated with any current modality continue to die of metastatic disease for years after treatment, indicating a systemic aspect to the course of uveal melanoma. Thus, high-risk patients could merit closer and or additional testing. In this study, we show that the use of machine learning classifiers such as the support vector machine can provide improved performance in identifying high-risk tumors. Also, within the framework of the ultrasound classification, different weightings or "costs" can be assigned to the false-positive and false-negative errors. This would allow both patient and physician to have a clearer understanding of the relative risk of various treatment options in terms of tumor risk category, treatment modality, and patient preferences, leading to more informed decision making.

In summary, this study demonstrated the ability of ultrasound backscatter analysis to detect noninvasively the presence of clinically significant prognostic features of uveal melanoma related to EMP patterns at a diagnostically significant rate. The ultrasound classification technique presented here can be used for patient stratification to different treatment modalities and to determine the frequency and type of clinical monitoring in light of assignment to high-risk or low-risk groups.

References

1. Singh AD, Shields CL, Shields JA. Prognostic factors in uveal melanoma. Melanoma Res 2001;11:255–63.
2. McLean IW, Foster WD, Zimmerman LE, Gamel JW. Modifications of Callender's classification of uveal melanoma at the Armed Forces Institute of Pathology. Am J Ophthalmol 1983;96:502–9.
3. Papadopoulos S, Benter T, Anastassiou G, et al. Assessment of genomic instability in breast cancer and uveal melanoma by random amplified polymorphic DNA analysis. Int J Cancer 2002;99:193–200.
4. Patel KA, Edmondson ND, Talbot F, et al. Prediction of prognosis in patients with uveal melanoma using fluorescene in situ hybridisation. Br J Ophthalmol 2001;85:1440–4.
5. Coleman DJ, Lizzi FL. Computerized ultrasonic tissue characterization of ocular tumors. Am J Ophthalmol 1983;96:165–75.
6. Coleman DJ, Rondeau MJ, Silverman RH, Lizzi FL. Computerized ultrasonic biometry and imaging of intraocular tumors for monitoring of therapy. Trans Am Ophthalmol Soc 1987; 85:49–81.
7. Goto H, Usui M, Ishii I. Efficacy of (123)N-isopropyl-p-[(123)I]-iodoamphetamine single photon emission computed tomography for the diagnosis of uveal malignant melanoma. Am J Ophthalmol 2001;132:937–9.
8. Lemke AJ, Hosten N, Bornfeld N, et al. Uveal melanoma: correlation of histopathologic and radiologic findings by using thin section MR imaging with a surface coil. Radiology 1999; 210:775–83.
9. Coleman DJ, Silverman RH, Rondeau MJ, et al. Correlations of acoustic tissue typing of malignant melanoma and histopathologic features as a predictor of death. Am J Ophthalmol 1990;110:380–8.
10. Coleman DJ, Silverman RH, Rondeau MJ, et al. Ultrasonic tissue characterization of uveal melanoma and prediction of patient survival after enucleation and brachytherapy. Am J Ophthalmol 1991;112:682–8.
11. Silverman RH, Folberg R, Boldt HC, et al. Correlation of ultrasound parameter imaging with microcirculatory patterns in uveal melanoma. Ultrasound Med Biol 1997;23:573–81.
12. Folberg R, Rummelt V, Parys-Van Ginderdeuren R, et al. The prognostic value of tumor blood vessel morphology in primary uveal melanoma. Ophthalmology 1993;100:1389–98.
13. Sakamoto T, Sakamoto M, Yoshikawa H, et al. Histologic findings and prognosis of uveal malignant melanoma in Japanese patients. Am J Ophthalmol 1996;121:276–83.
14. McLean IW, Keefe KS, Burnier MN. Uveal melanoma: comparison of the prognostic value of fibrovascular loops, mean of the ten largest nucleoli, cell type, and tumor size. Ophthalmology 1997;104:777–80.
15. Seregard S, Spångberg B, Juul C, Oskarsson M. Prognostic accuracy of the mean of the largest nucleoli, vascular patterns, and PC-10 in posterior uveal melanoma. Ophthalmology 1998;105:485–91.
16. Makitie T, Summanen P, Tarkkanen A, Kivela T. Microvascular loops and networks as prognostic indicators in choroidal and ciliary body melanomas. J Natl Cancer Inst 1999;91:359–67.
17. Maniotis AJ, Folberg R, Hess A, et al. Vascular channel

formation by human melanoma cells in vivo and in vitro: vasculogenic mimicry. Am J Pathol 1999;155:739–52.
18. Maniotis AJ, Chen X, Garcia C, et al. Control of melanoma morphogenesis, endothelial survival, and perfusion by extracellular matrix. Lab Invest 2002;82:1031–43.
19. Folberg R, Hendrix MJ, Maniotis AJ. Vasculogenic mimicry and tumor angiogenesis. Am J Pathol 2000;156:361–82.
20. Clarijs R, Otte-Höller I, Ruiter DJ, de Waal RM. Presence of a fluid-conducting meshwork in xenografted cutaneous and primary human uveal melanoma. Invest Ophthalmol Vis Sci 2002;43:912–8.
21. Pötgens AJ, van Altena MC, Lubsen NH, et al. Analysis of the tumor vasculature and metastatic behavior of xenografts of human melanoma cell lines transfected with vascular permeability factor. Am J Pathol 1996;148:1203–17.
22. Shirakawa K, Kobayashi H, Heike Y, et al. Hemodynamics in vasculogenic mimicry and angiogenesis of inflammatory breast cancer xenograft. Cancer Res 2002;62:560–6.
23. Mueller AJ, Freeman WR, Schaller UC, et al, Munich/San Diego/Iowa City Collaboration. Complex microcirculation patterns detected by confocal indocyanine green angiography predict time to growth of small choroidal melanocytic tumors: MuSIC Report II. Ophthalmology 2002;109:2207–14.
24. Lizzi FL, Greenebaum M, Feleppa EJ, et al. Theoretical framework for spectrum analysis in ultrasonic tissue characterization. J Acoust Soc Am 1983;73:1366–73.
25. Insana MF. Ultrasonic imaging of microscopic structures in living organs. Int Rev Exp Pathol 1996;36:73–92.
26. Folberg R, Pe'er J, Gruman LM, et al. The morphologic characteristics of tumor blood vessels as a marker of tumor progression in primary human uveal melanoma: a matched case-control study. Hum Pathol 1992;23:1298–305.
27. Folberg R, Verdick R, Weingeist TA, Montague PR. The gross examination of eyes removed for choroidal and ciliary body melanomas. Ophthalmology 1986;93:1643–7.
28. Montague PR, Meyer M, Folberg R. Technique for the digital imaging of histopathologic preparations of eyes for research and publication. Ophthalmology 1995;102:1248–51.
29. Folberg R, Fleck M, Mehaffey MG, et al. Mapping the location of prognostically significant microcirculatory patterns in ciliary body and choroidal melanomas. Pathol Oncol Res 1996;2:229–36.
30. Mehaffey MG, Folberg R, Meyer M, et al. Relative importance of quantifying area and vascular patterns in uveal melanomas. Am J Ophthalmol 1997;123:798–809.
31. Feleppa EJ, Lizzi FL, Coleman DJ, Yaremko MM. Diagnostic spectrum analysis in ophthalmology: a physical perspective. Ultrasound Med Biol 1986;12:623–31.
32. Lizzi FL, Astor M, Feleppa EJ, et al. Statistical framework for ultrasonic spectral parameter imaging. Ultrasound Med Biol 1997;23:1371–82.
33. Lizzi FL, Ostromogilsky M, Feleppa EJ, et al. Relationship of ultrasound spectral parameters to features of tissue microstructure. IEEE Trans Ultrason Ferroelectr Freq Control 1987;33:319–29.
34. Coleman DJ, Lizzi FL, Silverman RH, et al. A model for acoustic characterization of intraocular tumors. Invest Ophthalmol Vis Sci 1985;26:545–50.
35. Kaiser G. A Friendly Guide to Wavelets. Boston: Birkhäuser; 1994.
36. Ruttiman UE, Unser M, Rawlings RR, et al. Statistical analysis of functional MRI data in the wavelet domain. IEEE Trans Med Imaging 1998;17:142–54.
37. Turkheimer FE, Brett M, Aston JA, et al. Statistical modeling of positron emission tomography images in wavelet space. J Cereb Blood Flow Metab 2000;20:1610–8.
38. Cristianini N, Shawe-Taylor J. An Introduction to Support Vector Machines and Other Kernel-Based Learning Methods. Cambridge, United Kingdom: Cambridge University Press; 2000.
39. Vapnik VN. The Nature of Statistical Learning Theory. 2nd ed. New York: Springer-Verlag; 1995.
40. Burges C, Crisp D. Uniqueness of the SVM solution. Adv Neural Inf Process Syst 1999;12:223–9.
41. Joachims T. Estimating the generalization performance of a SVM efficiently. In: Langley P, ed. Proceedings of the Seventeenth International Conference on Machine Learning (ICML 2000). San Francisco: Morgan Kaufman; 2000:431–8.
42. Zhang T. Generalization performance of some learning problems in Hilbert functional spaces. Adv Neural Inf Process Syst 2001;14:543–50.
43. Macmillan NA, Creelman CD. Detection Theory: A Users Guide. Cambridge, United Kingdom: Cambridge University Press; 1991.
44. Provost F, Fawcett T. Analysis and visualization of classifier performance: comparison under imprecise class and cost distributions. In: Heckerman D, Mannila H, Pregibon D, Uthurusamy R, eds. Proceedings of the Third International Conference of Knowledge Discovery and Data Mining. Menlo Park, CA: AAAI Press; 1997:43–8 KDD-97.
45. Provost F, Fawcett T. Robust classification for imprecise environments. Machine Learn 2001;42:203–31.
46. Collaborative Ocular Melanoma Study Group. The COMS randomized trial of iodine 125 brachytherapy for choroidal melanoma. II: Characteristics of patients enrolled and not enrolled. COMS Report No. 17. Arch Ophthalmol 2001;119:951–65.
47. Collaborative Ocular Melanoma Study Group. The COMS randomized trial of iodine 125 brachytherapy for choroidal melanoma. III: initial mortality findings. COMS Report No. 18. Arch Ophthalmol 2001;119:969–82.
48. Shields JA, Shields CL, Ehya H, et al. Fine-needle aspiration biopsy of suspected intraocular tumors. The 1992 Urwick Lecture. Ophthalmology 1993;100:1677–84.
49. Folberg R, Augsburger JJ, Gamel JW, et al. Fine-needle aspirates of uveal melanomas and prognosis. Am J Ophthalmol 1985;100:654–7.
50. Augsburger JJ, Shields JA, Folberg R, et al. Fine needle aspiration biopsy in the diagnosis of intraocular cancer: cytologic-histologic correlations. Ophthalmology 1985;92:39–49.
51. Char DH, Kroll SM, Stoloff A, et al. Cytomorphometry of uveal melanoma: comparison of fine needle aspiration biopsy samples with histologic sections. Anal Quant Cytol Histol 1991;13:293–9.
52. DeMay RM. The Art and Science of Cytopathology. Vol. 1. Exfoliative Cytology. Chicago: ASCP Press; 1996.
53. Mehaffey MG, Gardner LM, Folberg R. Distribution of prognostically important vascular patterns across multiple levels in ciliary body and choroidal melanomas. Am J Ophthalmol 1998;126:373–8.
54. Barinaga M. A face off over tumor blood supply. Science 2000;287(5454):783, 785.
55. Hall CS, Scott MJ, Lanza GM, et al. The extracellular matrix is an important source of ultrasound backscatter from myocardium. J Acoust Soc Am 2000;107:612–9.
56. Coleman DJ, Silverman RH, Ursea R, et al. Ultrasonically induced hyperthermia for adjunctive treatment of intraocular malignant melanoma. Retina 1997;17:109–17.